



## Research Paper

# The phase response and state space of slow wave contractions in the small intestine

Sean P. Parsons  and Jan D. Huizinga 

*Farncombe Family Digestive Health Research Institute, McMaster University, Hamilton, Ontario, Canada*

Edited by: Mark Frey

## New Findings

- **What is the central question of this study?**  
What are the dynamical rules governing interstitial cell of Cajal (ICC)-generated slow wave contractions in the small intestine, as reflected in their phase response curve and state space?
- **What is the main finding and its importance?**  
The phase response curve has a region of phase advance surrounding a phase delay peak. This pattern is important in generating a stable synchrony within the ICC network and is related to the state space of the ICC; in particular, the phase delay peak corresponds to the unstable equilibrium point that threads the ICC's limit cycle.

Interstitial cells of Cajal (ICCs) generate electrical oscillations in the gut. Synchronization of the ICC population is required for generation of coherent electrical waves ('slow waves') that cause muscular contraction and thereby move gut content. The phase response curve (PRC) is an experimental measure of the dynamical rules governing a population of oscillators that determine their synchrony and gives an experimental window onto the state space of the oscillator, its dynamical landscape. We measured the PRC of slow wave contractions in the mouse small intestine by the novel combination of diameter mapping and single pulse electrical field stimulation. Phase change ( $\tau$ ) was measured as a function of old phase ( $\phi$ ) and distance from the stimulation electrode ( $d$ ). Plots of  $\tau(\phi, d)$  showed an arrowhead-shaped region of phase advance enclosing at its base a phase delay peak. The phase change mirrored the perturbed pattern of contraction waves in response to a pulse. The  $(\phi, d)$  plane is the surface of a displacement tube extending from the limit cycle through state space. To visualize the state space vector field on this tube, latent phase ( $\phi_{\text{lat}}$ ) was calculated from  $\tau$ . At the transition from advance to delay, isochrons made boomerang turns before tightening and winding around the phase delay peak corresponding to the unstable equilibrium point that threads the limit cycle. This isochron foliation had previously been observed in oscillator models such as the Fitzhugh–Nagumo but has not been demonstrated experimentally. The spatial extension of the PRC afforded by diameter mapping allows a better understanding of the dynamical properties of ICCs and how they synchronize as a population.

(Received 22 March 2017; accepted after revision 29 June 2017; first published online 3 July 2017)

**Corresponding author** S. P. Parsons: Farncombe Family Digestive Health Research Institute, McMaster University, 1280 Main Street West, HSC 3N4, Hamilton, ON, Canada L8S 4K1. Email: sparsonslab@gmail.com

## Introduction

Any physiological system is driven by many interdependent variables, which one may call the system's 'state variables' (Garfinkel, 1983; Strogatz, 2015). For example, in an electrically excitable cell, such as a heart muscle cell, the state variables would include membrane potential ( $V$ ) and intracellular calcium concentration ( $[Ca^{2+}]_i$ ). If both  $V$  and  $[Ca^{2+}]_i$  oscillate together (Fig. 1A), then plotting  $V$  against  $[Ca^{2+}]_i$  will trace a loop (Fig. 1B). The two-dimensional area of this plot is the 'state space' of the heart cell, i.e. each state variable is an axis of state space and state space has as many dimensions as there are state variables. The loop is the cell's 'trajectory' through state space. Another name for state space is 'phase space' (Nolte, 2010).

If the heart cell is given a short electrical stimulus, it will be displaced, probably along the  $V$  axis, to a new point in state space (Fig. 1C). The trajectory then winds back towards the loop it made before the stimulus, i.e. it returns to its previous oscillation. Given that the displaced trajectory returns to the loop in the mathematical 'limit' of time going to infinity, the loop is called a 'limit cycle'. At several points on the trajectory's return to the limit cycle, plot with an arrow its speed (rate of change of  $V$  and  $[Ca^{2+}]_i$ ), by the arrow's length, and direction (relative rate of change of  $V$  and  $[Ca^{2+}]_i$ ; Fig. 1D). Then give the cell more stimuli at different times, so that it is displaced to various points in state space, and again measure the trajectory speeds and directions as they return to the limit cycle. The resulting set of speeds and directions is the 'vector field' of the state space (Fig. 1E).

The vector field gives an overall picture of the dynamics of the heart cell without plotting individual trajectories. The field winds around to a point at the centre of the limit cycle where the speed (arrow length) goes to zero. This point is called an 'unstable equilibrium' because if the cell is displaced to this exact point oscillations will stop completely, but with the slightest push from this point (for instance due to environmental noise) the trajectory will wind back to the limit cycle.

Another way of picturing state space dynamics is with isochrons (Glass & Winfree, 1984). Instead of measuring trajectory speed and direction, measure the time taken to reach some fixed point on the limit cycle from each displaced point. Then plot the contours of this time; these are the isochrons (Fig. 1F). The closer together the isochrons, the slower the trajectory, i.e. there is an inverse relationship between the spacing of isochrons and vector field speed (the exact relationship is eqn (2)).

A mathematical model of a system may consist of a set of differential equations; specifically, one first-order ordinary differential equation (ODE) for each state variable that

gives the variable's rate of change as a function of one or more of the complete set of state variables and some constants (parameters) (Garfinkel, 1983). The state space vector field can be calculated directly from these ODEs. In an experiment, one cannot usually measure all the state variables, usually just one, and so one cannot measure the vector field. But one can measure the isochrons, the time taken to return to some point in the oscillation, irrespective of what state variable is measured. This makes isochrons a powerful experimental tool.

If its trajectory does not depart significantly from a limit cycle, a system can be described by a single ODE for its position on the limit cycle, its phase, rather than by a set of ODEs, one for each state variable (Levinson, 1950; Winfree, 1967). This ODE is a 'phase equation', and its greater simplicity allows faster computer simulation and easier mathematical analysis. For a pair of interacting oscillators, if each can only slow or speed up the progress of the other around its limit cycle, but not push it off its limit cycle, then each oscillator can be described by a phase equation consisting of only three components: the speed at which the oscillator would progress on its limit cycle without interaction (its natural frequency), the strength of interaction and an interaction function that describes how much to speed up or slow down depending on the phase difference between oscillators (Schwemmer & Lewis, 2012). The coupled phase equations constitute a 'weakly coupled oscillator model'. Here, 'weak coupling' refers specifically to the fact that the oscillators do not push each other off their limit cycles.

The phase response curve (PRC) measures the response of an oscillator to a short stimulus. It is the plot of the change in the oscillator's phase as a function of the phase at which the stimulus was given. The PRC has a long history in circadian rhythms and the heart beat (Glass & Winfree, 1984). For much of that history, its significance was more or less technical. It could be used to control rhythms. An electrical stimulus given at the right phase of the heart's oscillation could induce arrhythmia or restore rhythmicity (Winfree, 1987). It was the insight of Arthur Winfree, summarized in his *The Geometry of Biological Time* (Winfree, 1980), that the PRC has a deeper significance that ties together isochrons, state space and the phase equation. He realized that the measurement of the PRC was equivalent to measuring isochrons, because both measure the time of return to an oscillation after displacement by a stimulus (Winfree, 1967; Guckenheimer, 1975; Glass & Winfree, 1984). Furthermore, the interaction function is simply a smoothed version of the PRC (Ermentrout & Rinzel, 1984; Kuramoto, 1984). Winfree's work catalysed the development, by him and others, of a coherent and powerful mathematical theory of the PRC, phase equations and state space (summarized by Schwemmer & Lewis, 2012). Nevertheless, PRCs are rarely measured outside of the circadian field and

then are rarely interpreted in relationship to state space dynamics.

Here, we measure the PRC, and thereby the state space isochrons, of the interstitial cells of Cajal (ICCs). The small intestine has rhythmic contractions that travel its length in waves (Parsons & Huizinga, 2015). The rhythm originates with a network of ICCs that runs the length of the intestine. The membrane potential of each ICC oscillates, and these electrical oscillations ('slow waves') spread out into the muscle and cause corresponding waves of contraction. We measure the PRC using the method of diameter mapping coupled with single pulse electrical field stimulation.

## Methods

### Ethical approval

All procedures were approved and carried out in accordance with regulations of the Animal Research Ethics Board (approval no. AUP 14-12-49) of McMaster University, following the guidelines and policy statements established by the Canadian Council on Animal Care and legislation as presented in the Animals for Research Act, Ontario (1980) and administered by the Ontario Ministry of Agriculture and Food. The authors acknowledge the ethical principles of *Experimental Physiology* and confirm that the study was conducted in compliance with the

animal ethics checklist as detailed by Grundy (2015). Fourteen-week-old, female CD1 mice were obtained from Charles River Laboratories (Sherbrooke, QC, Canada) and fed *ad libitum* on standard chow. To obtain intestines, 14 mice were killed by cervical dislocation after induction of general anaesthesia with isoflurane, following an approved standard operating procedure of the Animal Research Ethics Board.

### Organ bath and diameter mapping

Lengths of small intestine were placed into an organ bath monitored by 10 video cameras for diameter mapping. Intestine preparation, the organ bath and camera apparatus were as described previously (Parsons & Huizinga, 2015) except for the following alterations. Instead of statically filling the intestine from a pressure reservoir (a Trendelenburg type apparatus), the lumen was continuously perfused. A Peri-Star Pro pump (World Precision Instruments, Sarasota, FL, USA) was used to pump oxygenated Krebs solution into the proximal end of the intestine at a rate of  $\sim 1.5 \text{ ml min}^{-1}$ . The inflow was warmed by passing the tube first through the bath. Outflow from the proximal end of the intestine was through Intramedic PE205 tubing (Becton Dickinson, Franklin Lakes, NJ, USA) passed through a hole in a rubber window at the end of the bath and into a

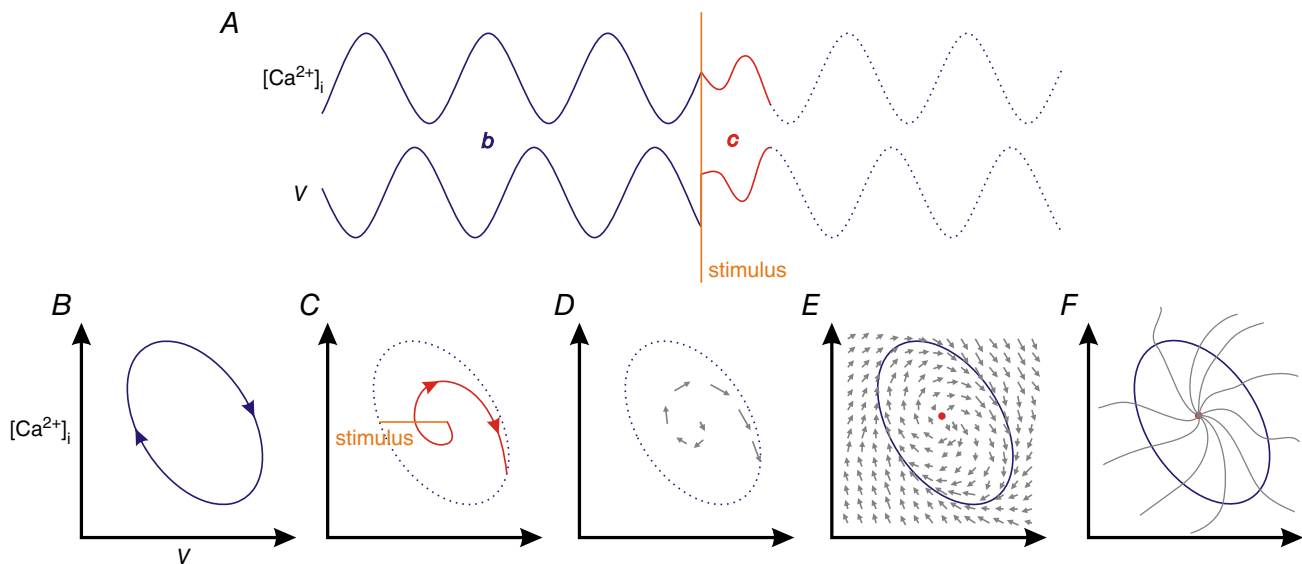


**Figure 1. State space**

A, intracellular calcium concentration ( $[\text{Ca}^{2+}]_i$ ) and membrane potential ( $V$ ) oscillations in a heart muscle cell or other 'excitable cell'. *b* and *c* refer to the blue and red trajectories in panel B and C, respectively. B, state space of the heart cell. A graphical plot of state space (also called phase space) is also known as a 'phase portrait'. The blue trajectory is the limit cycle of the heart cell. C, an electrical stimulus is given that displaces the cell along the  $V$  axis (orange). The trajectory then winds back to the limit cycle (red). D, vector representation of the return trajectory. E, the state space vector field. The central red point is the unstable equilibrium. Note that other arrangements of equilibria (stable and unstable) are possible (Strogatz, 2015). F, isochrons radiating out from the unstable equilibrium.

beaker. Instead of a 'kit-kat' intestine holder with five 0.5-cm-wide lanes, we used one with three 1-cm-wide lanes (Fig. 2). Instead of two aqualifter pumps, the bath solution was circulated by a brushless submersible micro pump (Docooler, Shenzhen, Guangdong, China). A plastic 'T' junction adaptor, perforated with a line of holes along the top edge and stoppered at the ends of the top edge, was attached to the outflow. This design was compact and gave a strong, approximately laminar flow. To prevent occasional luminal air bubbles lifting the intestine out of the lane, a criss-cross ladder of 40- $\mu$ m-diameter actuator wire (Dynalloy, Tustin, CA, USA), strung between two rods, was placed over the kit-kat (Fig. 2).

Diameter maps (Dmaps) were calculated from video recordings with custom ImageJ (US National Institutes of Health, Bethesda, MD, USA) plugins, as described previously (Parsons & Huizinga, 2015). Briefly, a Dmap was calculated for each camera, and the Dmaps were then stitched together by matching their edges. A set of plugins ('DMapLE') for Dmap creation and stitching can be freely downloaded from the website of S.P.P., [www.scepticalphysiologist.com/code/code.html](http://www.scepticalphysiologist.com/code/code.html).

### Electrical field stimulation

All experiments were carried out in the presence of 0.5 mM lidocaine to block neural activity. The central lane of the kit-kat held an intestine (Fig. 2). A pair of electrodes pointed down along opposing inside edges of the central lane, held in place by posts made of plastic tubing that squeeze fitted into the outer lanes (Fig. 2). An electrode consisted of 6 mm of exposed 0.2-mm-diameter platinum wire connected to a wire lead with heat-shrink-sealed junction. The intestine was held taut enough so that it ran

along the centre of the lane, not touching the electrodes. A tendency to bend meant that sometimes small blocks had to be placed in the lane to push the intestine towards the centre of the electrode pair. The leads of an electrode pair were connected to a Grass S48 stimulator (Natus, Pleasanton, CA, USA).

To record stimulation, an electroluminescent (EL) wire (Lerway, Shenzhen, Guangdong, China) was positioned along the length of the kit-kat, at one side just within the frame of the cameras (Fig. 2) and connected to a Grass stimulator. The sync-out port of this 'control' stimulator was wired to the sync-in ports of two 'slave' stimulators, each connected to a pair of stimulation electrodes. The slave stimulators had their repeat mode set to off, so that they fired a pulse only in response to the control stimulator, with the pulse amplitude and duration set by the slave itself. In this way, the EL wire and both stimulation electrode pairs were synchronized, but could be adjusted independently for pulse duration and amplitude. The control stimulator was set to 60 V (enough to light the EL wire), 300 ms duration (comfortably longer than the video frame interval of 33 ms) and a 0.02 Hz frequency or 50 s interval (long enough to allow the contraction pattern to re-equilibrate between pulses). The slave stimulators were set to either 50 or 80 V and 15 or 30 ms duration.

Parallel with Dmap calculation, for each frame a rectangular area over the EL wire was averaged along the direction orthogonal to the wire (and the kit-kat and intestine). This produced a stimulation map (Smap) showing the lighting of the EL wire. Stimulation times were detected in the Smap by a simple threshold algorithm (greater than the mean plus a multiple of the SD of the background).

### Phase response curve

A custom ImageJ plugin was written to calculate phase response curves from a Dmap. For each pulse, a rectangular region of interest (ROI) of  $18\text{ s} \times 5\text{ cm}$  was made, covering 2.5 cm each side of the electrode position and from 13.5 s before stimulation to 4.5 s after. The plugin first applied a median filter to the ROI using the ImageJ 'Remove Outliers' command with a radius of six pixels (0.48 mm, 180 ms) and threshold of 2, both bright and dark filtering. This removed speckles caused by bubbles generated at the electrodes and picked up by the diameter mapping algorithm. The plugin then found contractions (diameter minima) within the ROI using a two-dimensional Gaussian derivative steerable filter, as described previously (Parsons & Huizinga, 2015). Within the ROI, for each pixel row along the spatial axis ( $d$ ) the following were calculated by the plugin (Fig. 5A): the average interval of all complete contraction cycles before stimulation ( $T$ ); the interval from the last contraction

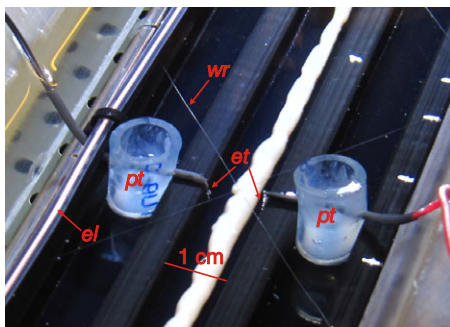


**Figure 2. Electrical field stimulation**

A pair of platinum wire electrodes (*et*) were positioned either side of the intestine, held in place by posts (*pt*) fitted in the outer lanes of the kit-kat. A criss-cross wire ladder (*wr*) was used to keep the intestine in the central lane if gas entered the lumen. Electroluminescent wire (*el*) lighted in synchrony with stimulation.



**Table 1. Gaussian components of the model phase response curve (eqn (1) and Fig. 9D)**

<i>a</i>	<i>c<sub>φ</sub></i>	<i>σ<sub>φ</sub></i>	<i>c<sub>d</sub></i>	<i>σ<sub>d</sub></i>
−0.45	0.6	0.17	0	0.4
−0.1	0.4	0.06	0	1
1.1	0.48	0.05	0	0.23
0.35	0.38	0.08	0	0.25

before stimulation to stimulation (phase at stimulation,  $\phi$ ); and the interval from the last contraction before stimulation to the next contraction (phase change,  $\tau$ ). Values of  $\phi$  and  $\tau$  were normalized to  $T$ .

Contour plots of  $\tau(\phi, d)$  were calculated in two stages. First, the vector of  $(\tau, \phi, d)$  samples was used to interpolate  $\tau$  values over a regularly spaced grid in the  $(\phi, d)$  plane using the MATLAB (MathWorks, Natick, MA, USA) function ‘meshgrid’ (0.05 spacing in  $\phi$ ; 0.2 cm spacing in  $d$ ). This grid was then converted to a contour map with the MATLAB function ‘contour’.

A model PRC was constructed from the superposition of four two-dimensional Gaussians, as follows:

$$\tau(\phi, d) = 1 + \sum_{j=1}^4 a_{(j)} \exp \left[ -\frac{(\phi - c_{\phi(j)})^2}{2\sigma_{\phi(j)}^2} - \frac{(d - c_{d(j)})^2}{2\sigma_{d(j)}^2} \right] \quad (1)$$

The model was fitted by eye to approximate an archetypal or average PRC, rather than by regression to a single PRC. Parameter values are given in Table 1. The added 1 at the left of the equation’s right-hand side follows from the definition of  $\tau = 1$  as refractory (see Results).

## Results

### Response to electrical field stimulation

In the presence of 0.5 mM lidocaine, to block neural activity, waves of contraction travelled distally along the small intestine. They had a stable velocity ( $\sim 1 \text{ cm s}^{-1}$ ) and frequency ( $\sim 0.8 \text{ Hz}$ ; Parsons & Huizinga, 2015), forming a regular pattern of diagonals in the Dmap (Fig. 3A). Single pulses of electrical field stimulation disturbed the wave pattern in a manner that varied widely from pulse to pulse (Fig. 3A). A contraction wave, as defined by a diameter minimum (red lines in Fig. 3), often terminated before reappearing along its natural line of propagation (dashed black lines in Fig. 3). At the termination or initiation point of a wave, its phase is singular (indeterminate), a phase singularity. Each pulse response was classified by an  $m:n$  number pair, where  $m$  was the number

of terminating singularities and  $n$  was the number of initiating singularities (upper right corner of each panel in Fig. 3A). Where  $m \neq n$ , either a wave terminated but did not reinitiate ( $m > n$ ) or a wave initiated where there was none before ( $m < n$ ). When either occurs, the unpaired singularity is called a dislocation, a term originating from crystallography;  $m - n$  is the topological charge or winding number of the dislocation (Berry, 1998).

There was never a simple, clean break in a wave such that the resulting two singularities remained opposed along the natural line of the wave (Fig. 3B). Instead, the wave sped up as it approached its terminating singularity, in the Dmap bending to the left from its natural line (Fig. 3C). The initiating singularity’s wave either remained on its natural line or was faster near its singularity, in the Dmap bending to the right of its natural line. There was therefore a lag between the singularities, and they would interdigitate (Fig. 3C). In dislocation responses (lower panels of Fig. 3A), the wave after the last terminating singularity sped up so much that it transferred onto the natural line of that singularity’s wave (Fig. 3C and D) to form the dislocation, and this transfer occurred across the next few waves until eventually the disturbance petered out. This was the reason for giving the pulses at such a low frequency (0.02 Hz, 50 s cycle<sup>−1</sup>), to allow the system to re-equilibrate after dislocation.

Six intestines were stimulated, each over four 20 min periods. Each period consisted of a maximum of 24 pulses (at 0.02 Hz) of the same amplitude and duration, applied synchronously at two electrode pairs separated by either 7 or 11 cm. The pulse amplitude and duration were one of the four possible permutations of 50 or 80 V amplitude and 15 or 30 ms duration. Therefore the total data consisted a maximum of 1152 pulse responses (6 intestines  $\times$  4 periods  $\times$  24 pulses  $\times$  2 electrode pairs). 1109 pulse responses were recorded and classed either by their  $m:n$  number or as ‘not equilibrated’ (NE) when there was a disturbance in the wave pattern before the pulse that made interpretation of the response impossible. This was either due to the nearby presence of spontaneous dislocations that occur at frequency steps (Parsons & Huizinga, 2015) or because the wave pattern had not re-equilibrated after the last pulse.

Apart from NE (23%), the dominant responses were 0:0 (32%) and 1:1 (20%). The rest of the response classes had frequencies of  $< 6\%$  (Fig. 4A). There was an increase in both the mean frequency of singularity ( $m > 0$ ) and dislocation ( $m > n$ ) responses with increasing pulse amplitude and duration (Fig. 4B and C), but these were not significant (none with  $P < 0.05$ ) as assessed by multiple Student’s paired  $t$  tests and two-way ANOVA. Of the 160 dislocation responses, all but six had a topological charge of  $+1$ . Those six were two 3:1, two 4:2, a 5:3 and a 3:0.

### Phase response curve

Three measurements were made for each pulse, for each point in the neighbourhood of the electrode, as follows (Fig. 5A): distance ( $d$ ) relative to the electrode ( $d = 0$ ); the interval from the last contraction before the pulse to the pulse (phase at pulse,  $\phi$ ); and the interval from the last contraction before the pulse to the next contraction (phase change,  $\tau$ ). Values of both  $\phi$  and  $\tau$  were normalized to  $T$ , the undisturbed contraction interval measured as the average of several full cycles before the pulse. Contraction waves always travelled distally, owing to the ICC natural frequency gradient (Parsons & Huizinga, 2015, 2016). Therefore as each contraction wave approached the pulse time,  $\phi$  decreased while  $d$  increased, generating a diagonal line of sample points across the ( $\phi$ ,  $d$ ) plane (Fig. 5B). The contraction wavelength ( $\lambda$ ) was the span of  $d$  covered by this line. Multiple waves, measured over many pulses, generated multiple lines that filled out the ( $\phi$ ,  $d$ ) plane in a diagonal, raster-like pattern (Fig. 5C). The set of points can be thought of as a function,  $\tau(\phi, d)$ , a spatial extension

of the more usual PRC,  $\tau(\phi)$  (see Fig. 1 of Parsons & Huizinga, 2016).

If  $\tau = 1$ , the oscillator is said to be refractory (the contraction has proceeded as if there were no pulse). If  $\tau < 1$ , the oscillator is phase advanced (the contraction has occurred earlier than it otherwise would). If  $\tau > 1$ , the oscillator is phase delayed (the contraction has occurred later than it otherwise would). The  $\tau(\phi, d)$  of one 20 min pulse period (Fig. 5C and D) had an arrowhead-shaped region of phase advance pointed along the  $\phi$  axis, symmetrical about  $d = 0$ , its base beginning at  $\phi = 0$  and its tip ending at approximately  $\phi = 0.75$ . The phase advance corresponded to the wave speeding up, so that it bent left in the map towards the pulse time (compare Fig. 5A and B). In the wedge at the arrowhead's base was a peak of phase delay at  $\phi \approx 0.2$  (Fig. 5C and D). Delay resulted from either the wave of the first initiating singularity 'bending right' from its natural line ( $\tau < 1 + \phi$ ) or a gap between the first terminating–initiating singularity pair ( $\tau > 1 + \phi$ ;  $\tau = 1 + \phi$  is 'full phase delay', the blue line in Fig. 5E and F).

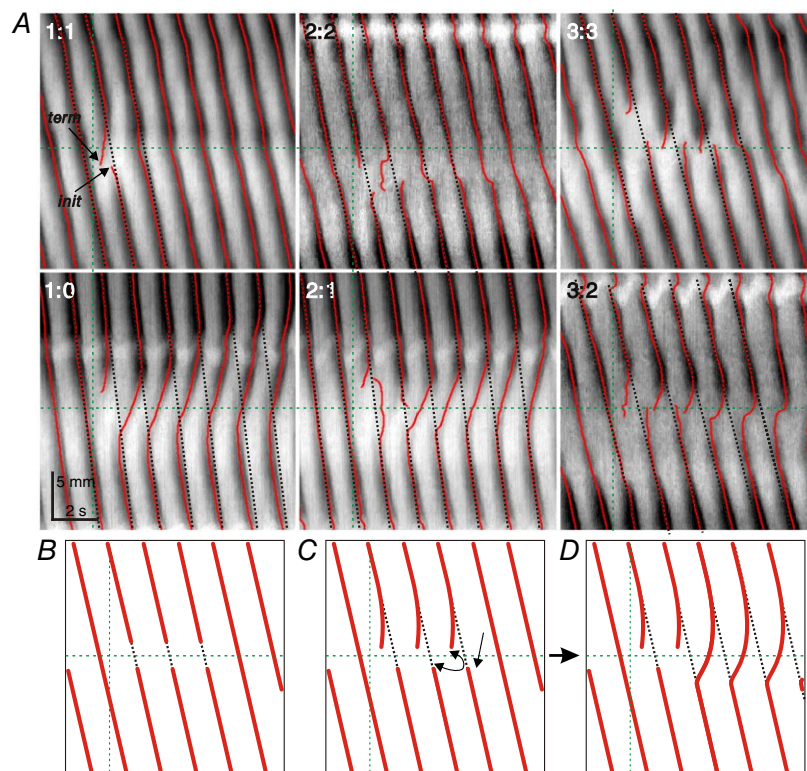


**Figure 3. Electrical field stimulation responses classed by singularity numbers**

A, example responses to single pulses of electrical field stimulation. Green dotted lines indicate the pulse time (vertical) and electrode position (horizontal). Red lines indicate detected contractions (diameter minima). Black dotted lines indicate 'natural lines' of contractions. Responses were classed as  $m:n$  (upper right corner of each panel), where  $m$  was the number of terminating contraction phase singularities (*term*) and  $n$  was the number of initiating singularities (*init*);  $m - n$  is the winding number or topological charge of the response. B, a 3:3 response formed by a clean break in contraction waves. C, a 3:3 response when the waves speed as they reach termination. D, a 2:1 response resulting when the last terminating wave of a 3:3 response advances onto the natural line of the wave before it.

When the PRC is used to calculate the interaction function for a weakly coupled oscillator model, the convention is that the start of the PRC ( $\phi = 0$ ) corresponds to the period of its maximal influence on another oscillator, the maximum of its impulse function. In bioelectrical oscillators, this is the period of membrane potential depolarization, the slow wave in ICC. As a result of the inactivation kinetics of the voltage-dependent ion channels that cause the depolarization, this period is also the refractory period of the oscillator. In our case, the

refractory period began after the phase advance tip at  $\phi \approx 0.75$ . This would suggest that depolarization begins a quarter of a cycle before maximal contraction (diameter minimum) at  $\phi = 0$ . To keep with convention, we shifted the  $\phi$  axis,  $\phi_{\Delta} = \text{mod}(\phi + 0.25, 1)$ , so that  $\tau(\phi_{\Delta}, d)$  shows the refractory period at the start of the cycle (compare Fig. 5E and F).

The PRC form varied considerably (Fig. 6). Phase delay varied from zero, where the responses were dominantly 0:0 (Fig. 6A) to  $\tau = 2$  with  $m > 0$  responses (Fig. 6B and C). The width of the phase advance arrowhead varied from 2 to 3 cm. In some cases, the arrowhead was asymmetrical, one arm having greater advance than the other (Fig. 6B). The more advanced arm was usually the distal ( $+d$ ), as the wave continued distal to the electrode without terminating, speeding ever more while  $\phi$  decreased, and so increasing phase advance (right-hand panel of Fig. 6B).

There was no apparent dependence of  $\tau(\phi_{\Delta}, d)$  on either the pulse duration or amplitude over the range we gave. For each pulse period (set of pulses of constant amplitude and duration), we calculated the mean  $\tau$  for all delayed points ( $\tau > 1.2$ ) and all advanced points ( $\tau < 0.8$ ; Fig. 7). There were no significant changes (none with  $P < 0.05$ ) in these means with pulse amplitude and duration, as assessed by multiple Student's paired  $t$  tests and two-way ANOVA.

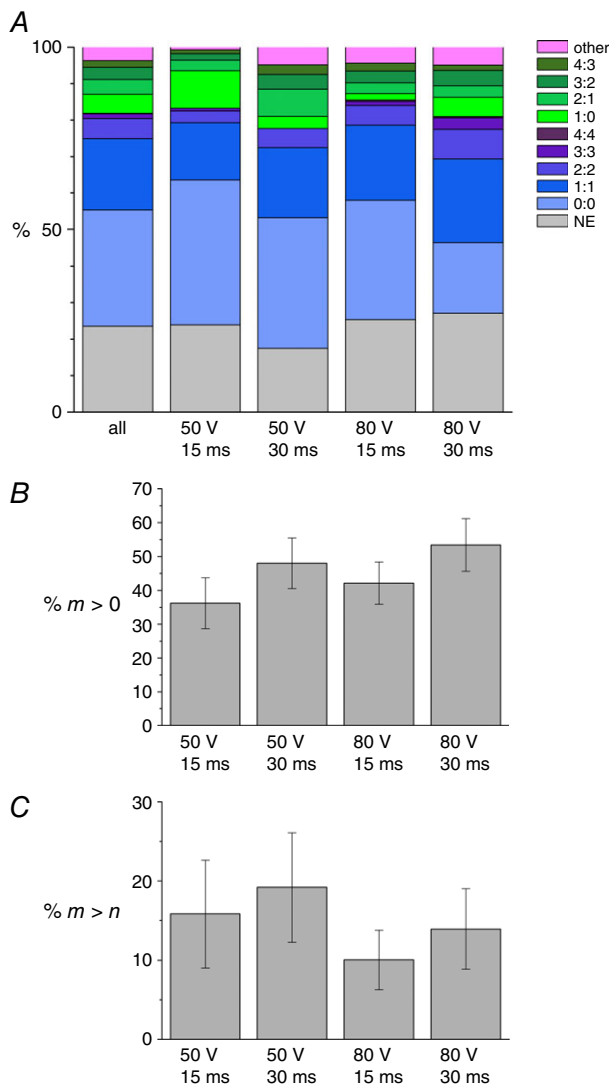


**Figure 4. Frequency of response classes**

A, percentage frequency of  $m:n$  response classes with aggregation according to pulse amplitude and duration. NE is non-equilibrated (response could not be classed because of a disturbed wave pattern before stimulation). 'Other' is any other  $m:n$  than those indicated. B, frequency of  $m > 0$  responses (all those with singularities). C, frequency of  $m > n$  responses (dislocations). Each bar in B and C is the mean  $\pm$  SEM of  $N = 12$  pulse periods.

## State space

A limit cycle has a basin of attraction, the part of state space where all trajectories eventually reach the limit cycle. For each point within the basin, one can define the 'latent' or 'asymptotic' phase,  $\phi_{\text{lat}}(\mathbf{x}) = 1 - (t \bmod 1)$ , where  $\mathbf{x}$  is the point's co-ordinate vector and  $t$  is the time taken by the trajectory from  $\mathbf{x}$  to the neighbourhood of some point  $\mathbf{x}'$  on the limit cycle, normalized by the period of the cycle, i.e.  $\phi_{\text{lat}}$  is a measure of the time taken from any point in state space to a specific point on the limit cycle. The importance of  $\phi_{\text{lat}}$  follows from the continuity equation (Kuramoto, 1984), as follows:

$$\frac{d\phi_{\text{lat}}}{dt} = 1 = \nabla\phi_{\text{lat}} \cdot \dot{\mathbf{x}} = \|\nabla\phi_{\text{lat}}\| \|\dot{\mathbf{x}}\| \cos\theta \quad (2)$$

The gradient of  $\phi_{\text{lat}}$  ( $\nabla\phi_{\text{lat}}$ ) is an inverse measure of the state space vector field ( $\dot{\mathbf{x}}$ ; Fig. 1E), and trajectories move up this gradient at a constant rate of ascent (of 1). The  $\phi_{\text{lat}}$  gradient can be visualized as isochrons,  $n - 1$  dimensional hypersurfaces of constant  $\phi_{\text{lat}}$ , where  $n$  is the number of dimensions of state space (Fig. 1F; Winfree, 1980; Glass & Winfree, 1984). By analogy to a geographical map, the isochrons are contours on a map of  $\phi_{\text{lat}}$ . A trajectory cuts across the isochrons (at an angle of  $\theta$  to their normal), and the more closely spaced the isochrons, the slower the trajectory (smaller  $\dot{\mathbf{x}}$ ). Isochrons are arranged



around the limit cycle like spokes on a wheel and converge at the unstable equilibrium that threads the cycle (Fig. 1*F*). But the spokes are rarely straight. They tend to twist and contort, often in a spiral pattern. This ‘foliation’ of isochrons is a unique fingerprint of the state space (Winfree, 1980; Langfield *et al.* 2014).

The PRC measures  $\phi_{\text{lat}}$  in the following manner. First an  $\mathbf{x}'$  neighbourhood is chosen that can be identified objectively in the experiment. In our case, this was the diameter minimum. Next, one uses a stimulus pulse to displace the trajectory from some point on the limit cycle

( $\mathbf{x}_L$ ) to some point off it ( $\mathbf{x}_D$ ). If, as in our case, the stimulus is electrical, the displacement will be predominantly along the axis of an electrical state variable, such as membrane potential. In terms of the PRC,  $\tau(\phi)$ , it follows that:

$$\phi_{\text{lat}}(\mathbf{x}_L) = \phi \quad (3)$$

$$\phi_{\text{lat}}(\mathbf{x}_D) = 1 - [(\tau - \phi) \bmod 1] \quad (4)$$

At a fixed displacement (stimulus strength) with varying  $\phi_{\text{lat}}(\mathbf{x}_L)$ ,  $\phi_{\text{lat}}(\mathbf{x}_D)$  is measured around a ring in state space,

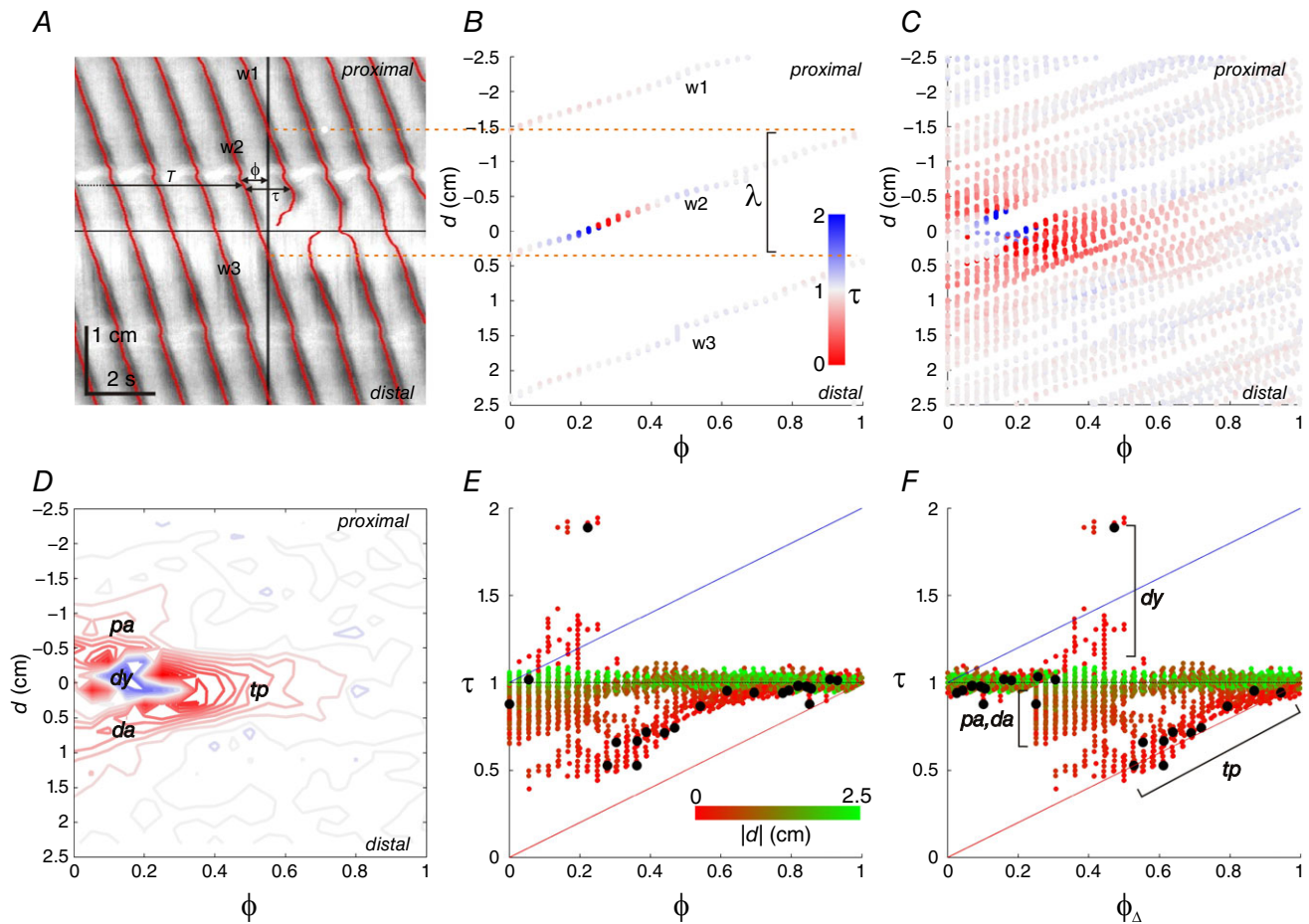


**Figure 5. Measurement of the phase response curve (PRC)**

A, Dmap showing the 1:1 response to an 80 V, 30 ms pulse. Vertical and horizontal black lines indicate the pulse time and electrode position, respectively. Red lines are diameter minima used to calculate  $\phi$  and  $\tau$  at each position along the spatial axis ( $d$ ). B, PRC.  $\tau$  is coded as the colour of each sample point in the  $(\phi, d)$  plane. Each contraction wave (w1, w2, w3) traces out a diagonal of points across  $(\phi, d)$  within the region of  $d$  where it is the last wave to precede the pulse (dotted orange lines for w2). This region corresponds to the cycle wavelength ( $\lambda$ ) at the pulse. C, PRC filled out by data from 22 more pulses of the same amplitude and duration. D,  $\tau(\phi, d)$  contour map calculated from the scatter plot (see Methods) with the same colour scale. The arrowhead-shaped region of phase advance (red contours) has a tip (tp) and two arms, proximal (pa) and distal (da). In the wedge between arms is a phase delay peak (dy). E, PRC.  $|d|$  is coded as the colour of each sample point in the  $(\phi, \tau)$  plane. Black dots are the points at  $d = 0$ . Red and blue lines indicate full phase advance and delay, respectively (see Fig. 1 of Parsons & Huizinga, 2016). F, PRC shifted along  $\phi$  to meet convention (see Results).



displaced from the limit cycle by  $\|\mathbf{x}_D - \mathbf{x}_L\|$ . Electrical field strength, and therefore displacement, decreases as the inverse square of distance from the electrodes (Coulomb's law), as follows:

$$\|\mathbf{x}_D - \mathbf{x}_L\| \approx |d|^{-2} \quad (5)$$

Thus  $\phi_{\text{lat}}(\mathbf{x}_D)$  is measured across the surface of a tube that extends out from the limit cycle, as distance from the

electrode decreases (Fig. 8A; see also Fig. 11, chapter 6 of Winfree, 1980). The  $(\phi, d)$  plane of the PRC is this tube cut along its length, opened flat and reflected along  $d = 0$  (Fig. 8B).

We transformed experimental  $\tau(\phi_\Delta, d)$  to  $\phi_{\text{lat}}(\phi_\Delta, -|d|)$  using eqn (4). To visualize isochrons (contours of  $\phi_{\text{lat}}$ ), we used a colour scale for  $\phi_{\text{lat}}$  that repeated over a set of rainbow colours. The isochrons then follow the bands

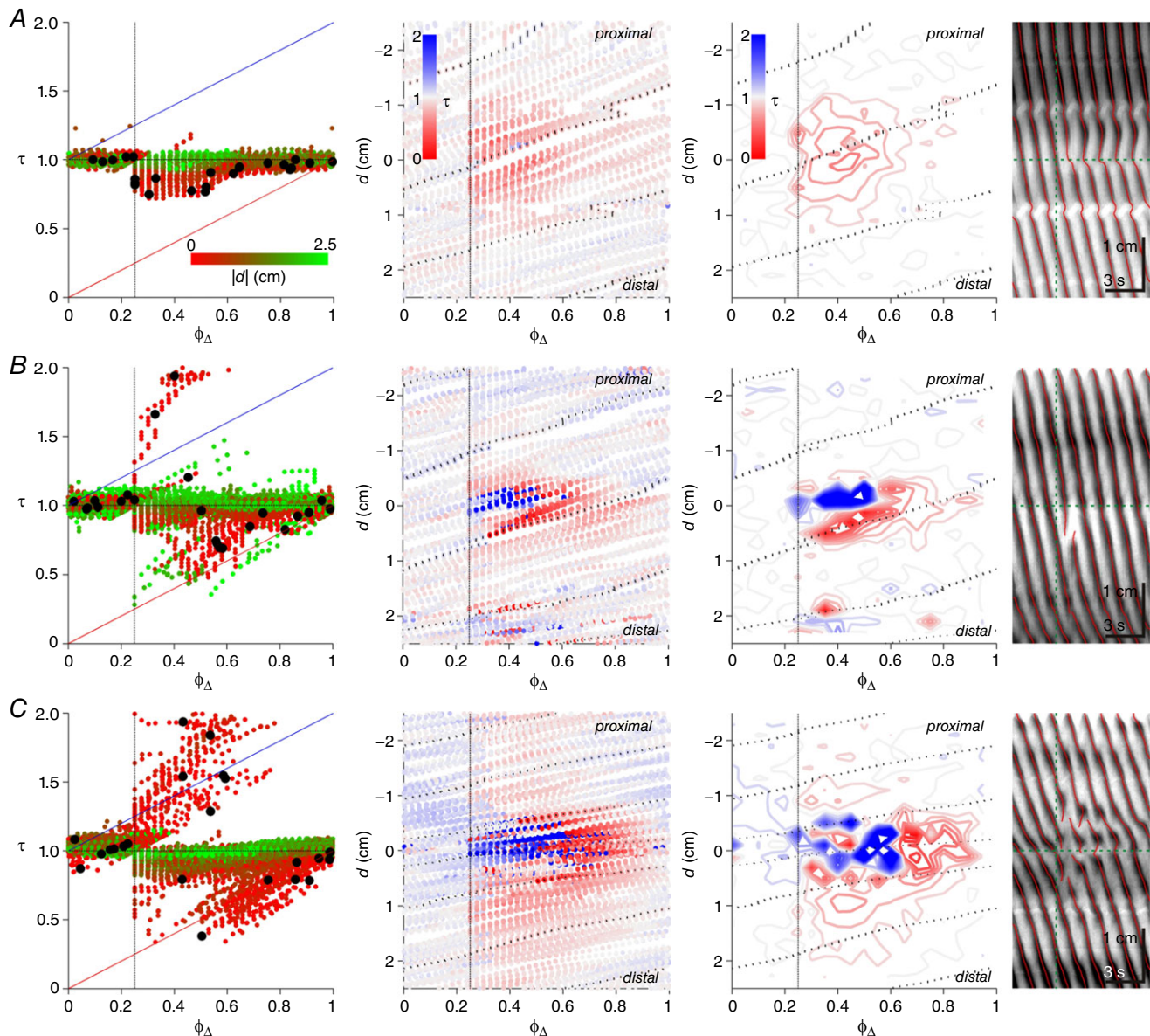


**Figure 6. Variation in PRCs**

Three PRCs from different intestines. *A*, phase advance only; 24 pulses at 80 V and 15 ms. *B*, asymmetrical phase advance arms; 23 pulses at 50 V and 15 ms. *C*, large phase delay; 23 pulses at 50 V and 30 ms. Far left,  $|d|$  coded as the colour of each sample point in the  $(\phi_\Delta, \tau)$  plane. Black dots are the points at  $d = 0$ . Vertical dotted lines indicate  $\phi = 0$ . Middle left,  $\tau$  coded as the colour of each sample point in the  $(\phi_\Delta, d)$  plane. Middle right, contour plots of the same. Far right, example Dmap responses. Red lines indicate detected contractions. Green horizontal and vertical dotted lines are the electrode position and pulse time, respectively.

of colour. This method was used by Winfree (Winfree, 1987). On the  $(\phi_\Delta, -|d|)$  plane, isochrons will twist to the left with phase advance [ $\phi_{\text{lat}}(\mathbf{x}_D) > \phi_{\text{lat}}(\mathbf{x}_L)$ ], to the right with phase delay [ $\phi_{\text{lat}}(\mathbf{x}_D) < \phi_{\text{lat}}(\mathbf{x}_L)$ ], and will be vertical when refractory. In the refractory region, isochrons were parallel with the  $d$ -axis (Fig. 9A–C). Near to the phase delay peak, isochrons twisted left, corresponding to the surrounding arms of the phase advance arrowhead (Fig. 9A–C). The experimental sample points were too noisy and not dense enough in the  $(\phi_\Delta, d)$  plane to make a clearer picture of state space on the displacement tube. This was especially true near to the phase delay peak, where points of divergent  $\tau$  or  $\phi_{\text{lat}}$  were clustered together. To gain a clearer understanding of the relationship of the PRC to state space, we made a model of the experimental  $\tau(\phi_\Delta, d)$  from the summation of four two-dimensional Gaussians (Fig. 9D). This was then transformed to  $\phi_{\text{lat}}(\phi_\Delta, -|d|)$ . The foliation was much clearer in the model (Fig. 9F). Isochrons twisted left at the arms of the phase advance arrowhead (Fig. 9E and F) and then twisted back right at the boundary with the phase delay peak. This back and forth twist of isochrons has been called a ‘boomerang turn’ by Osinga & Moehlis (2010). The isochrons twisted close together about the phase delay peak itself, indicative of slow trajectories. Osinga & Moehlis (2010) called this much denser region of isochrons the ‘slow manifold’.

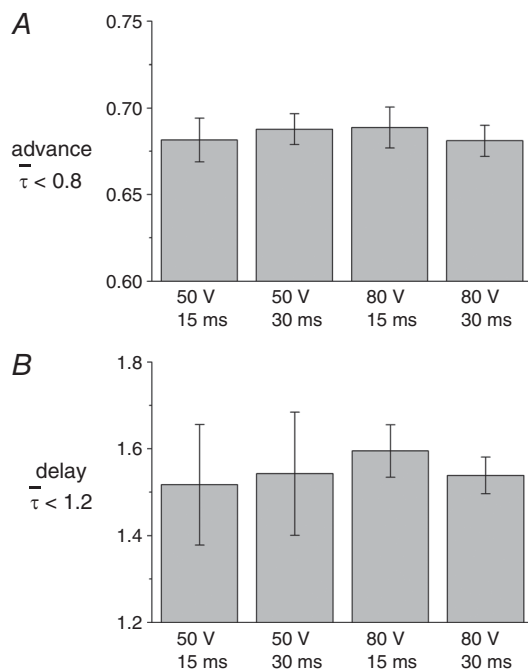


**Figure 7. Phase response curve amplitude and pulse amplitude and duration**

A, mean of PRC points  $\tau < 0.8$  (phase advance). B, mean of PRC points  $\tau > 1.2$  (phase delay). Each bar is the mean  $\pm$  SEM of  $N = 12$  pulse periods.

## Discussion

We have measured the PRC of ICC using the novel approach of diameter mapping combined with electrical field stimulation. The PRC consisted of a refractory region, followed by phase delay, followed by phase advance. This shape is reflected in the contraction response to a single pulse, which can be classed by the wave singularities generated. The PRC provides a window onto the state space of ICC and has significant physiological implications, as discussed below.

## Physiology of the PRC

The shape of the ICC PRC (refractory, followed by delay, followed by advance) seems to be ubiquitous in nature. It is seen in the PRCs of circadian oscillations of diverse species, the heart beat and the Krebs cycle (Winfree, 1980). As Pavlidis (1973) has remarked, ‘it turns out that most curves obtained experimentally belong to a small subset of all possible shapes of PRCs’. There is a good reason for this. Biological rhythms are commonly generated by a population of synchronized, oscillatory

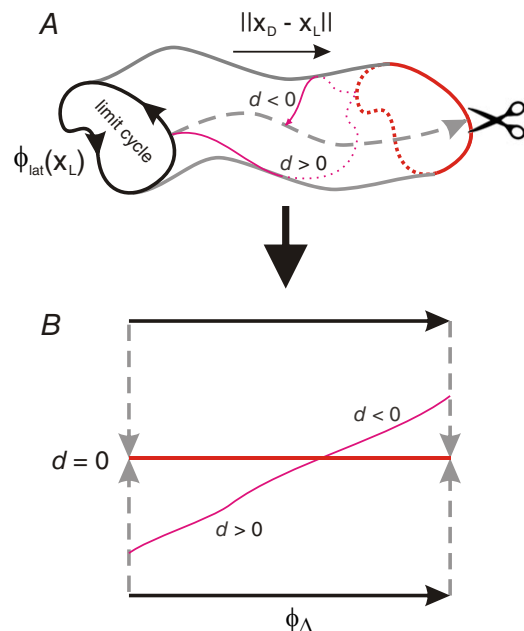


**Figure 8. The displacement tube and the PRC**

A, the displacement tube extends out from the limit cycle along the axis of displacement. The tube might not be straight because of non-linearities in the system. In our experiment, maximal displacement (red ring) is at zero distance from the electrode ( $d = 0$ ). B, the  $(\phi, d)$  plane of the PRC is the displacement tube cut along  $\phi_{\text{lat}}(\mathbf{x}) = 0$  (dashed grey lines), unfurled and reflected along  $d = 0$  (red line; compare with Fig. 5B). A single contraction wave traces out a line of sample points (pink line) that screws once around the displacement tube's circumference and is reflected where it crosses  $d = 0$ .





This is an example of an allometric law (biological scaling relationship), of which there are many (West *et al.* 1997). Dawson (2014) has made a detailed derivation of the allometric law of heart rate, but we are not aware of anyone who has studied the theoretical underpinning of refractory period scaling, nor are we aware of any allometric studies of the intestine slow wave, but from our mouse data compared with the rabbit it appears that a similar relationship holds to the heart for both cycle length and refractory period. The cycle length in the mouse intestine was 1.2–1.5 s as against 3–4 s in the rabbit (Cheung & Daniel, 1980).

In the mouse, the end of the refractory period ( $\phi_{\Delta} = 0.25$ ) was coincident with maximal contraction (minimal diameter). In gastric muscle preparations when slow waves were recorded by intracellular electrode, simultaneously with contraction, it was found that contraction rises through the depolarization and reaches a maximum at the return to resting potential (Szurszewski, 1975; see also Lammers, 2005). It appears to be the general case for transient cellular depolarization (any ‘action potential’) that the return to resting potential is coincident with the end of the refractory period. It follows by syllogism that the end of the slow wave refractory period should be coincident with maximal contraction, in agreement with our data.

The state space vector field, and thus PRC shape, is determined by the properties of the ion channels expressed by the ICCs, their kinetics and dependence on voltage and second messengers, such as intracellular calcium. For instance, the refractory period of an action potential (slow wave in ICCs) ends as the depolarizing (inward current-generating) ion channels leave inactivation. In Hodgkin–Huxley type cell models (see next section), the PRC shape can be altered by changing the activation kinetics and reversal potentials of ion channels (Tsumoto *et al.* 2006; Izhikevich, 2007). Imtiaz *et al.* (2006) measured the PRC of an ICC model cell that had the same refractory–delay–advance shape as our experimental PRC. However, they did not show the effect of parameter changes, other than stimulus strength, on PRC shape.

### State space

The Hodgkin–Huxley model of the squid axon action potential has provided the template for a family of models of electrically ‘excitable’ cells. One ODE (state variable) for membrane potential ( $V$ ) summates the current contributions from one or more Ohmic ion channels ( $dV/dt = \Sigma I/C$  where  $I$  is channel current and  $C$  is membrane capacitance). The other state variables are the voltage-dependent gating (activation or inactivation) variables for these ion channels and have non-linear ODEs. The Hodgkin–Huxley model has two voltage-dependent ion channels, with three gating

variables and thus a four-dimensional state space. The Morris–Lecar model also has two voltage-dependent channels, but only one gating variable. One channel reaches activation instantaneously. This reduction of the state space dimension to two is very useful for analysis and visualization of the state space. Dimension reduction can also be achieved by abstraction of the Hodgkin–Huxley template. Instead of describing Ohmic channels, the  $V$  ODE is a polynomial with a cubic  $V$  term. The cubic term reproduces the non-linearity of the gating variables of the Hodgkin–Huxley template, as reflected in the cubic  $V$ -nullcline (the line through state space where  $dV/dt = 0$ ). The gating variable ODEs are themselves linear. Such abstracted membrane models include the Fitzhugh–Nagumo and Hindmarsh–Rose.

Both Hodgkin–Huxley and abstracted models produce oscillations over large ranges of parameter values (regions of their parameter space). Winfree computed the isochrons for a limit cycle in the Fitzhugh–Nagumo (Box C, Chapter 6 of Winfree, 1980). As the isochrons converged on the unstable equilibrium, they twisted into a complex spiral of interdigitating, petal-like folds. With modern computing power, Osinga and colleagues have mapped the equilibrium point foliation in much greater detail for both the Fitzhugh–Nagumo (Langfield *et al.* 2014) and a Hodgkin–Huxley template model (Osinga & Moehlis, 2010). Winfree held out the possibility that the ‘ornate structure of isochrons near their convergence point [might] provide an experimental distinction between such oscillators’ (Box D, Chapter 6 of Winfree, 1980). However, he pointed out that this distinction could be difficult to discern owing to the density of the foliation structure, variation between samples and the noise and imprecision inherent in experimental measurement. This is born out by our results (Fig. 9C). Nevertheless, the grosser isochron structure, away from the equilibrium point, can still provide a rough constraint to model building. In comparison to the model PRC, it is clear that the unstable equilibrium point corresponds to the centre of the phase delay peak.

The equilibrium point was called by Winfree the ‘blackhole’, because if the trajectory is brought to this point by a pulse, then oscillations will stop. This could be one explanation for why contraction waves broke into singularities, the gap between them being where oscillators ‘disappeared into the hole’ (Fig. 3). The stopped ICCs restarted only because they are coupled and so could be restarted by their still oscillating neighbours. An alternative explanation is that the oscillators in the gap were still oscillating but in a region close about the equilibrium point and below contraction threshold ( $V$  needs to go above a certain value for contraction of the muscle), from which the trajectory took a long time to escape. We cannot find any explanation for why either of these mechanisms would select between giving an  $m = n$



response or a dislocation. Perhaps this has more to do with the coupling between oscillators.

The success of our weakly coupled oscillator model of the intestine (Parsons & Huizinga, 2016) in modelling contraction waves in the absence of neural activity suggests that the ICCs do not leave their limit cycle in these conditions. It is possible that neural stimuli may force ICCs off their limit cycle and so produce gaps in contraction waves or dislocations, due to trajectories pushed onto the slow manifold about the equilibrium point. Both gaps and dislocations are seen experimentally in the absence of neural block by lidocaine (S.P. Parsons and J.D. Huizinga, unpublished data). Dislocations are also seen in the presence of neural blockade (Parsons & Huizinga, 2015, 2016), associated with frequency steps, and so can certainly arise from trajectories confined to the limit cycle. Both frequency-step-associated and neurally evoked dislocations should not be considered as ‘ectopic pacemakers’ of pathophysiological significance, but rather the natural consequence of the dynamics of coupled ICCs.

### Type I or II

In some cases, there was no phase delay peak (Fig. 6A) corresponding to a type I PRC. Different shapes of PRCs can result from different models or model parameters. For the latter, it is typical to talk in terms of what bifurcation the model is near. A bifurcation is a change in the numbers or types of equilibria points or cycles, brought about by a change in parameters, that qualitatively changes the behaviour of the system (Strogatz, 2015). Hansel and Ermentrout have suggested that the type II PRC is characteristic of a limit cycle with parameters near to a supercritical Andronov–Hopf bifurcation and the type I PRC is near to a saddle node on invariant circle bifurcation (Hansel *et al.* 1995; Ermentrout, 1996). This could be the case here. Some regions of the intestine may be near different bifurcations owing to variation in some physiological parameter, perhaps a channel reversal potential. However, the simpler explanation for the lack of a phase delay peak is that in these cases displacement was not big enough to reach near the equilibrium point. Where there was a phase delay peak, it was surrounded at smaller displacement (greater distance from the electrode) by the arms of the phase advance arrowhead. In cases without the phase delay peak, it is reasonable to assume that maximal displacement was less, and so these arms are all that were seen.

Recognizing that the  $\tau(\phi)$  PRC shape depends on the amount of displacement from the limit cycle is important when modelling. In our weakly coupled oscillator model, we used an interaction function with only phase advance, according to the PRC of Cheung and Daniel (1980). This was the correct choice, as the interaction function is supposed to reflect the PRC at infinitesimal displacement

from the limit cycle (the oscillators are weakly coupled) and our data show that at this displacement phase is only advanced.

### Coupling and PRC measurement

The coupling between ICCs is both the necessity of our experiment and its major limitation. Without coupling there would be no contraction waves and so nothing to measure. With contraction waves, as opposed to recording slow waves from a single point (Cheung & Daniel, 1980), one can measure the PRC at different distances from the electrode and so measure over a displacement tube rather than at a single displacement. However, the PRC should be measured ideally for a single, uncoupled oscillator if one wants to know the state space or interaction function of that individual oscillator. Following displacement by the pulse, ICCs will inevitably influence each other in their trajectory back to the limit cycle. This should be a small effect, for a number of reasons. First, the success of the weakly coupled oscillator model of intestinal waves (Parsons & Huizinga, 2016) indicates that ICCs are weakly coupled. If they cannot strongly perturb each other from their limit cycles, then they are unlikely to have a strong effect on each other's trajectories off the limit cycle. Second, the strength of interaction between oscillators is reflected in the time scale over which those oscillators will synchronize or desynchronize and so form patterns. It took the disturbance caused by electrical field stimulation over half a minute to re-equilibrate, hence the 50 s we gave between pulses. Measurements of  $\tau$  were made within 1.5 s of the pulse. Third, neighbouring ICCs start off near each other on the limit cycle and so should be displaced to the same point and mostly follow each other back to the limit cycle. Any displacement from the uncoupled trajectory will be attributable to longer range coupling, which decays quickly.

Phase response curves have not become a standard experimental tool outside of the circadian rhythm field (Castellanos *et al.* 1984; Goldberg *et al.* 2007). One reason for this could be the high degree of precision required in the presence of instrumental and environmental noise typical of biological systems. This problem increases at shorter time scales. Precision is high for circadian scales, but for neural oscillators, with millisecond intervals, PRCs may be almost lost in the noise (Goldberg *et al.* 2007). Our experimental system and time scale appear to be slightly above the threshold to obtain reliable information about dynamics and state space.

### Summary

The PRC is a picture of the state space of an oscillator, revealing its dynamics. It can be used to guide biophysical models and used directly in weakly coupled oscillator

models via the interaction function. As far as we are aware, we are the first to have measured a PRC continuously over different displacements, and thus experimentally measured an isochron structure and foliation, since Winfree's 'pinwheel experiment' on *Drosophila* pupa emergence (Winfree, 1980). The shape of the ICC PRC, refractory followed by phase delay and advance, is common to most biological oscillators, reflecting an evolutionary convergence on dynamical principles that allow for synchronization within an oscillator population.

## References

- Berry MV (1998). Much ado about nothing: optical dislocation lines (phase singularities, zeros, vortices). *Proc. SPIE* **3487**, 1–5.
- Castellanos A, Luceri RM, Moleiro F, Kayden DS, Trohman RG, Zaman L & Myerburg RJ (1984). Annihilation, entrainment and modulation of ventricular parasystolic rhythms. *Am J Cardiol* **54**, 317–322.
- Cheung DW & Daniel EE (1980). Comparative study of the smooth muscle layers of the rabbit duodenum. *J Physiol* **309**, 13–27.
- Dawson TH (2014). Allometric relations and scaling laws for the cardiovascular system of mammals. *Systems* **2**, 168–185.
- Ermentrout B (1996). Type I membranes, phase resetting curves, and synchrony. *Neural Comput* **8**, 979–1001.
- Ermentrout GB & Rinzel J (1984). Beyond a pacemaker's entrainment limit: phase walk-through. *Am J Physiol Regul Integr Comp Physiol* **246**, R102–R106.
- Garfinkel A (1983). A mathematics for physiology. *Am J Physiol Regul Integr Comp Physiol* **245**, R455–R466.
- Glass L & Winfree AT (1984). Discontinuities in phase-resetting experiments. *Am J Physiol Regul Integr Comp Physiol* **246**, R251–R258.
- Goldberg JA, Deister CA & Wilson CJ (2007). Response properties and synchronization of rhythmically firing dendritic neurons. *J Neurophysiol* **97**, 208–219.
- Grundy D (2015). Principles and standards for reporting animal experiments in *The Journal of Physiology and Experimental Physiology*. *Exp Physiol* **100**, 755–758.
- Guckenheimer J (1975). Isochrons and phaseless sets. *J Math Biol* **1**, 259–273.
- Hansel D, Mato G & Meunier C (1995). Synchrony in excitatory neural networks. *Neural Comput* **7**, 307–337.
- Imtiaz MS, Katnik CP, Smith DW & van Helden DF (2006). Role of voltage-dependent modulation of store  $\text{Ca}^{2+}$  release in synchronization of  $\text{Ca}^{2+}$  oscillations. *Biophys J* **90**, 1–23.
- Izhikevich EM (2007). *Dynamical Systems in Neuroscience*. MIT Press, Cambridge, MA.
- Janse MJ, Opthof T & Kleber AG (1998). Animal models of cardiac arrhythmias. *Cardiovasc Res* **39**, 165–177.
- Kuramoto Y (1984). *Chemical Oscillations, Waves and Turbulence*. Springer-Verlag, Berlin.
- Lammers WJ (2005). Spatial and temporal coupling between slow waves and pendular contractions. *Am J Physiol Gastrointest Liver Physiol* **289**, G898–G903.
- Langfield P, Krauskopf B & Osinga HM (2014). Solving Winfree's puzzle: the isochrons in the FitzHugh-Nagumo model. *Chaos* **24**, 013131.
- Levinson N (1950). Small periodic perturbations of an autonomous system with a stable orbit. *Ann Math* **52**, 727–738.
- Nolte DD (2010). The tangled tale of phase space. *Physics Today* **63**, 33–38.
- Osinga HM & Moehlis J (2010). Continuation-based computation of global isochrons. *Siam J Appl Dyn Syst* **9**, 1201–1228.
- Parsons SP & Huizinga JD (2015). Effects of gap junction inhibition on contraction waves in the murine small intestine in relation to coupled oscillator theory. *Am J Physiol Gastrointest Liver Physiol* **308**, G287–G297.
- Parsons SP & Huizinga JD (2016). Spatial noise in coupling strength and natural frequency within a pacemaker network; consequences for development of intestinal motor patterns according to a weakly coupled phase oscillator model. *Front Neurosci* **10**, 19.
- Pavlidis T (1973). *Biological Oscillators: their Mathematical Analysis*. Academic Press, New York.
- Schwemmer MA & Lewis TJ (2012). The theory of weakly coupled oscillators. In *Phase Response Curves in Neuroscience*, ed. Schultheiss NW, Prinz AA & Butera RJ, pp. 3–31. Springer, New York.
- Strogatz SH (2015). *Nonlinear Dynamics and Chaos*. Westview Press, Boulder, CO.
- Szurszewski JH (1975). Mechanism of action of pentagastrin and acetylcholine on the longitudinal muscle of the canine antrum. *J Physiol* **252**, 335–361.
- Tsumoto K, Kitajima H, Yoshinaga T, Aihara K & Kawakami H (2006). Bifurcations in Morris–Lecar neuron model. *Neurocomputing* **69**, 293–316.
- West GB, Brown JH & Enquist BJ (1997). A general model for the origin of allometric scaling laws in biology. *Science* **276**, 122–126.
- Winfree AT (1967). Biological rhythms and the behavior of populations of coupled oscillators. *J Theor Biol* **16**, 15–42.
- Winfree AT (1980). *The Geometry of Biological Time*. Springer-Verlag, Heidelberg.
- Winfree AT (1987). *The Timing of Biological Clocks*. Freeman, New York.

## Additional information

### Competing interests

None declared.

### Author contributions

This work was carried out in the laboratory of J.D.H. at the Farncombe Institute, McMaster University. S.P.P. conceived, designed, carried out and analysed the experiments. J.D.H. contributed to the conception of the work and critically revised the manuscript. Both authors approved the final version of

the manuscript and agree to be accountable for all aspects of the work in ensuring that questions related to the accuracy or integrity of any part of the work are appropriately investigated and resolved. Both persons designated as authors qualify for authorship, and all those who qualify for authorship are listed.

### Funding

This study was supported by Canadian Institutes of Health Research grant MOP12874; Natural Sciences and Engineering Research Council grant 386877; and a research support grant from the Farncombe Family Digestive Diseases Research Institute.